Neurobiology of Disease

Rapamycin Delays Disease Onset and Prevents PrP Plaque Deposition in a Mouse Model of Gerstmann–Sträussler–Scheinker Disease

Constanza J. Cortes, Kefeng Qin, Julie Cook, Ani Solanki, and James A. Mastrianni
Department of Neurology, The University of Chicago Pritzker School of Medicine, Chicago, Illinois 60637

Autophagy is a cell survival response to nutrient deprivation that delivers cellular components to lysosomes for digestion. In recent years, autophagy has also been shown to assist in the degradation of misfolded proteins linked to neurodegenerative disease (Ross and Poirier, 2004). In support of this, rapamycin, an autophagy inducer, improves the phenotype of several animal models of neurodegenerative disease. Our Tg(PrP-A116V) mice model Gerstmann–Sträussler–Scheinker disease (GSS), a genetic prion disease characterized by prominent ataxia and extracellular PrP amyloid plaque deposits in brain (Yang et al., 2009). To determine whether autophagy induction can mitigate the development of GSS, Tg(PrP-A116V) mice were chronically treated with 10 or 20 mg/kg rapamycin intraperitoneally thrice weekly, beginning at 6 weeks of age. We observed a dose-related delay in disease onset, a reduction in symptom severity, and an extension of survival in rapamycin-treated Tg(PrP-A116V) mice. Coincident with this response was an increase in the autophagy-specific marker LC3II, a reduction in insoluble PrP-A116V, and a near-complete absence of PrP amyloid plaques in the brain. An increase in glial cell apoptosis of unclear significance was also detected. These findings suggest autophagy induction enhances elimination of misfolded PrP before its accumulation in plaques. Because ataxia persisted in these mice despite the absence of plaque deposits, our findings also suggest that PrP plaque pathology, a histopathological marker for the diagnosis of GSS, is not essential for the GSS phenotype.

Introduction

Autophagy is a cell survival mechanism whereby cellular components are phagocytized by double membrane autophagosomes that transport cargo to lysosomes for degradation. Initially recognized as a cellular response to nutrient deprivation, autophagy has since been shown to participate in the clearance of aggregate-prone cytosolic proteins linked to a variety of neurodegenerative disorders (Ross and Poirier, 2004). Autophagy is negatively regulated by the mammalian target of rapamycin (mTOR) (Schmelzle and Hall, 2000). Rapamycin is a lipophilic macrolide antibiotic (Noda and Ohsumi, 1998) that inhibits mTOR and potently induces autophagy. Numerous reports describe protective effects of rapamycin in cell, fly, and mouse models of several neurodegenerative diseases that result from accumulation of misfolded aggregate-prone cytosolic proteins, including Parkinson's disease (PD) (Webb et al., 2003), amyotrophic lateral sclerosis (Fornai et al., 2008), Huntington's disease (HD) (Berger et al., 2006), spinocerebellar ataxia (Ravikumar et al., 2002, 2004), and frontotemporal dementia (Williams et al., 2006). Despite the lack of cytosolic aggregates in Alzheimer's disease (AD), autophagy appears to play a complex role in Aβ production and clearance, and recent work suggests a beneficial effect of rapamycin in some AD mouse models (Nixon, 2007; Spilman et al., 2010; Yang et al., 2011).

Prion diseases are transmissible neurodegenerative disorders linked to accumulation of misfolded pathogenic isoforms (PrP^{Sc}) of normal prion protein (PrP^{C}) (Prusiner, 1998). Pharmacologic induction of autophagy appears to promote the clearance of PrP^{Sc} *in vitro* (Heiseke et al., 2009a,b), and a limited number of *in vivo* studies have found either no effect (Sarkar et al., 2007) or a modest effect (Heiseke et al., 2009b) to prolong survival following scrapie infection. However, whether autophagy induction can delay the development of genetic prion disease has not been addressed.

Gerstmann–Sträussler–Scheinker disease (GSS) is a genetic prion disease, typified by the onset of progressive ataxia and the presence of PrP amyloid plaque deposits in brain, a feature reminiscent of AD. We previously constructed the Tg(PrP-A116V) transgenic mouse line that recapitulates the major clinicopathologic features of GSS, notably the onset of progressive ataxia and accumulation of thioflavin S-positive PrP amyloid plaques, especially within the cerebellum (Yang et al., 2009).

To determine whether autophagy functions in genetic prion disease and amyloid plaque pathology, we chronically treated Tg(PrP-A116V) mice with rapamycin, beginning at 6 weeks of age. We report a dose-dependent delay in disease onset, symptom

Received Dec. 13, 2011; revised July 11, 2012; accepted July 20, 2012.

Author contributions: C.J.C. and J.A.M. designed research; C.J.C., K.Q., J.C., and A.S. performed research; A.S. contributed unpublished reagents/analytic tools; C.J.C., K.Q., and J.A.M. analyzed data; C.J.C., K.Q., and J.A.M. wrote the paper.

This work was supported by NIH Grant R01NS051480 and The Brain Research Foundation (J.A.M.).

The authors declare no competing financial interests.

Correspondence should be addressed to Dr. James A. Mastrianni, Prion Laboratory, Department of Neurology, MC2030, University of Chicago Pritzker School of Medicine, 5841 South Maryland Avenue, Chicago, IL 60637. E-mail: jmastria@uchicago.edu.

C. J. Cortes's present address: Department of Pediatrics, University of California, San Diego, San Diego, CA 92037.

J. Cook's present address: Indiana University School of Medicine Northwest, Gary, IN 46408.

DOI:10.1523/JNEUROSCI.6189-11.2012

 0270-6474/12/3212396-10$15.00/0

severity, and improved survival of rapamycin-treated Tg(PrP-A116V) mice. These improvements were accompanied by an increase of the specific autophagy marker LC3II in brain, a reduction in insoluble PrP-A116V, a near-total absence of PrP amyloid plaques, and interestingly, but of unclear significance, an increase in glial cell apoptosis.

Our results suggest a role for autophagy in genetic prion disease and extracellular plaque generation, and they support autophagy induction as a potential therapeutic approach. The conspicuous absence of plaque pathology yet persistence of ataxia, albeit with reduced severity, supports the concept that PrP amyloid plaque deposits, while pathognomonic for GSS, are not required for the GSS phenotype.

Materials and Methods

Transgenic mice

The Tg(PrP-A116V) mice have been described previously (Yang et al., 2009). In short, the A116V mutation and 128V polymorphism were introduced into the mouse *Prnp* coding segment by site-directed mutagenesis, ligated into the XhoI-cut MoPrP.Xho vector (ATCC JHU-2; American Type Culture Collection), and injected into pronuclei of fertilized eggs from PrP knock-out [Tg($Prnp^{o/o}$)] parental mice at the University of Chicago Transgenic Mouse Facility. A founder that expressed approximately four to six times normal mouse PrP were bred to Tg($Prnp^{o/o}$) mice, so they express only the mutated mouse PrP-A116V/128V protein. Male and female mice were used randomly throughout the study.

Rapamycin injections

Rapamycin (Sirolimus; LC Laboratories) was dissolved in pure ethanol as a 20 mg/ml stock solution and diluted in injection buffer (4% ethanol, 5% Tween 80, 5% PEG400 in dH_2O) on the day of injection to a dose of 10 or 20 mg/kg in a final volume of ~0.1 ml. Mice were weighed weekly throughout the experiment, and dosages were adjusted accordingly. Control mice received a similar volume of injection buffer without active drug. Beginning at 6 weeks of age, injections were administered intraperitoneally Monday, Wednesday, and Friday, until killed for analysis.

Clinical assessment

At the start of the treatment, mice were monitored daily for typical signs of prion disease, including gait ataxia, roughened fur, hunched posture, and poor righting reflex. We developed a detailed clinical assessment scale to monitor the progression of disease. Since ataxia and mobility problems are key features of this mouse model, these features are heavily weighted in the assessment. The following scoring from A0 to A6 is used: A0, no ataxia; A0/1, no ataxia, but may show other signs such as rough fur or walking lower to the ground; A1, more consistent, but still a subtle change in gait (wider, lower to ground), but not definitive ataxia; A1/A2, subtle but definite wobble that is intermittent; A2, persistent and obvious wobble—this stage defines the clear onset of ataxia; A3, stumble/loss of footing occasionally (once or twice during a 2 min observation); A4, stumble/loss of footing every few steps; mouse may occasionally start to sway (rock back and forth) when in a stationary position; A4/A5, early-stage A5, with brief spells of falling to one side and more swaying; A5, falling nearly constantly, weight loss generally obvious, clear change in coat roughness; A6, lethargic, very hunched, emaciated. Mice are generally killed during stage A5 or early in A6 (A5/A6), as they can no longer feed and death is imminent. Ataxia typically develops at ~130–140 d of age.

PrP analysis

Western blots. Fresh frozen brain was used to prepare 10% (w/v) brain homogenates in lysis buffer (20 mM Tris-HCl, pH 7.4, 150 mM NaCl, 1 mM EDTA, 0.5% Triton X-100, 0.5% Na-deoxycholate). Brain homogenate (5 or 2%) was separated by SDS-PAGE on a 14% gel. Following electrophoresis, samples were transferred to polyvinylidene difluoride membranes (Bio-Rad) that were washed in TBST (20 mM Tris-HCl, 0.9% NaCl, 0.1% Tween 20, pH 7.6), blocked for 1 h with 5% milk, washed, and incubated in TBST with 1% milk containing anti-mouse PrP antibodies D13 (InPro) at 1:3000 or SAF32 (SPI Bio) at 1:200, or antibodies for LC3B (Cell Signaling) at 1:1000, or α-tubulin (Santa Cruz) at 1:10,000, all incubated overnight at 4°C. After washing, secondary antibodies (anti-human-HRP for D13, anti-mouse-HRP for SAF32, and α-tubulin) were added at concentrations from 1:5000 to 1:2000. Blots were imaged with West Pico ECL (Thermo Fisher Scientific) and captured with a Bio-Rad Alpha Document Imager. Densitometry quantifications were performed using NIH ImageJ or TotalLab TL100 software (TotalLab).

Solubility assay. Brain homogenates were prepared in lysis buffer. A fraction was removed for analysis and centrifuged at 4°C for 1 h at 100,000 × *g* in a Sorvall RC M120EX ultramicrocentrifuge, using a RP100-AT4 rotor. The pellet was washed once with lysis buffer, centrifuged, and resuspended in the starting volume of lysis buffer containing 1% SDS. Equal supernatant and pellet fractions were subjected to Western blotting and densitometry analysis, as above.

Histological studies

Cerebellum sections. Mice were asphyxiated with CO_2 and slowly perfused via cardiac puncture with 20 ml of PBS followed by 20 ml of 4% paraformaldehyde (Sigma-Aldrich). Brains were stored in 4% paraformaldehyde for 48 h and then transferred to PBS containing 0.1% sodium azide (Sigma-Aldrich) until paraffin embedding. The blocks of mouse cerebella were cut at similar landmarks of the cerebellum into 5 μm coronal sections. Sections were depariffinized with xylene (Thermo Fisher Scientific) immediately before staining.

Thioflavin S staining. Sections were stained with 0.05% thioflavin S (Sigma-Aldrich) for detection of PrP amyloid deposits and with 10 μg/ml 4′,6-diamidino-2-phenyl-indole, dihydrochloride (DAPI) (Invitrogen) to visualize nuclei, and then observed with a Zeiss Axioplan fluorescence microscope at excitation wavelength of 520 nm for thioflavin S and 450 nm for DAPI. Plaque burden was calculated as the area of thioflavin S staining per area of entire cerebellar section, using NIH ImageJ. Several sections were analyzed from each group to obtain the mean area of thioflavin S staining per cerebellar area for each treatment group. The average fraction of plaque area per cerebellar area of the 160-d-old vehicle-treated mice was normalized to a value of 100, with which all other groups were compared. The data are presented as the relative plaque burden. The absolute plaque counts were zero in all sections examined in mice receiving rapamycin at 20 mg/kg.

Terminal deoxynucleotidyl transferase-mediated biotinylated UTP nick end labeling. DNA fragmentation was assessed with the terminal deoxynucleotidyl transferase-mediated biotinylated UTP nick end labeling (TUNEL) apoptosis detection kit (Millipore), following the manufacturer's instruction. Briefly, sections were incubated with proteinase K for 30 min. After incubation with a reaction mix containing biotin-dUTP and the terminal deoxynucleotidyl transferase (TdT) for 60 min, sections were incubated with the avidin–FITC solution for 30 min in the dark. As positive control, the fixed sections were incubated with 5 μg/ml DNase I in PBS for 60 min at 37°C before labeling following the manufacturer's instruction. Sections treated with the TdT reaction mix containing no TdT were used as negative controls. For nuclear staining, sections were incubated with 10 μg/ml DAPI (Sigma-Aldrich) at room temperature for 1 min. Sections were washed with PBS, air dried, mounted, and observed with a Zeiss Axioplan fluorescence microscope at excitation wavelength of 520 nm for FITC and 450 nm for DAPI. For quantitative analysis of apoptosis, the percentage area of TUNEL-positive signal relative to the area of DAPI stain in each cerebellar section was calculated, using NIH ImageJ, and the mean determined and plotted.

Immunofluorescence of NeuN and GFAP. Brain sections were first TUNEL stained, with the proteinase K step eliminated, blocked with 2% BSA in PBS for 1 h, and then incubated with rabbit anti-glial fibrillary acidic protein (GFAP) antibody (1:100) (Dako) or mouse anti-NeuN antibody (1:50) (Millipore Bioscience Research Reagents) overnight. DyLight 649-conjugated AffiniPure goat anti-rabbit or mouse IgG, F(ab′) was used as secondary antibody. Results were visualized by a fluorescence microscopy and verified under a confocal microscope (BX61; Olympus).

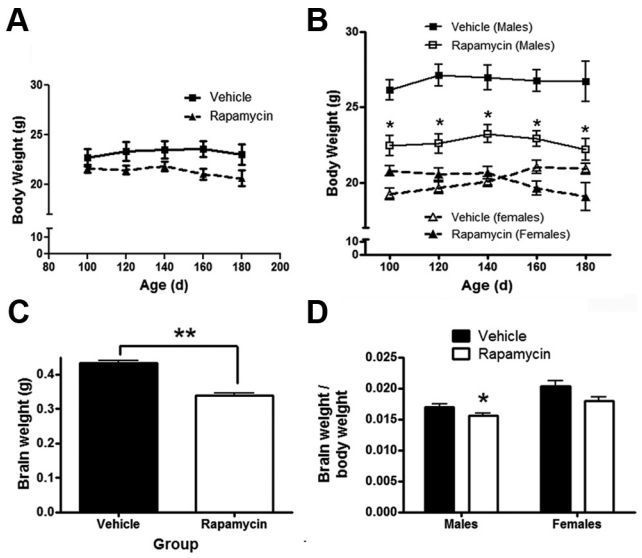

Figure 1. Rapamycin reduces weight gain in male Tg(PrP-A116V) mice. ***A***, Average weight ± SE, in grams, of all mice treated with rapamycin at 20 mg/kg or vehicle from 6 weeks of age, measured between 100 (presymptomatic) and 180 (symptomatic) days of age ($n = 12$ per group). No significant differences at any time point. ***B***, Data from ***A***, but separated by gender. Males (squares) and females (triangles) treated with rapamycin, compared with vehicle-treated, mice within the same gender group. Rapamycin-treated males weighed significantly less than vehicle-treated males at the start of the weight recordings, suggesting reduced weight gain with the initiation of rapamycin. *$p < 0.05$, Student's *t* test, measured at each time point. Data from mice receiving 10 mg/kg rapamycin are not shown, to simplify the figure, but no statistical difference compared with 20 mg/kg was detected. ***C***, Brain weight (in grams) from ~160-d-old male and female Tg(PrP-A116V) mice treated with vehicle or rapamycin at 20 mg/kg ($n = 16$ each, 10 males, 6 females). **$p < 0.001$, Student's *t* test. ***D***, Ratio of brain to body weight in 160-d-old Tg(PrP-A116V) male and female mice treated with vehicle or rapamycin at 20 mg/kg ($n = 6$ each). *$p = 0.0496$, Student's *t* test.

Semiquantitative RT-PCR

Brains of Tg(PrP-A116V) mice treated with rapamycin (0, 10, or 20 mg/kg) were harvested and quick frozen at −80°C. Total RNA was extracted using the RNAqueous-4PCR kit (Ambion). A total of 500 ng of RNA from each sample was used for RT-PCR using SuperScript One-Step RT-PCR with Platinum Tag (Invitrogen) to synthesize cDNA of mouse PrP and LC3. β-Actin was used as control. The PCR primers were designed as follows: mouse PrP^C, forward, 5′-TGG GGA CAA CCT CAT GGT GGT, and reverse, 5′-GAT ATT GAC GCA GTC GTG CAC-3′ (expected PCR product, 329 bp), mouse LC3, forward, 5′-TTC AAG CAG CGG CGC ACG TTC-3′, and reverse, 5′-CTC CTC TTG ACT CAG AAG CCG AAG GTT-3′ (expected PCR product, 360 bp), mouse β-actin, forward, 5′-TGG AAT CCT GTG GCA TCC ATG AAA-3′, and reverse, 5′-TAA AAC GCA GCT CAG TAA CAG TCC G (expected PCR product, 348 bp). The PCR products were separated on a 1% 1× Tris-acetate EDTA (Tris-acetate EDTA)-agarose gel and analyzed on a document imaging system (Bio-Rad). Densitometric analysis was performed using NIH ImageJ. The mean signal of PrP and LC3 cDNA from three experiments each were normalized to β-actin cDNA, and the relative percentage change in PrP or LC3 mRNA among the three treatment groups was reported.

Results

Rapamycin impairs weight gain of Tg(PrP-A116V) mice

Prior work suggests that rapamycin impairs weight gain in rodents (Walpoth et al., 2001; Ravikumar et al., 2004). To assess for this possibility in Tg(PrP-A116V) mice, weight measurements were recorded weekly from a presymptomatic period of 100 d. When assessed as a group, mice treated with rapamycin at 20 mg/kg had similar weights as vehicle-treated mice over the entire monitoring period (Fig. 1*A*); however, when separated by gender, there were differences. From the beginning of the weight assessment period and at each time point thereafter, males receiving either dose of rapamycin weighed less than vehicle-treated males (Fig. 1*B*). This suggests an initial reduction in weight gain from the start of injections at 6 weeks until the start of the recording period at 100 d, but no differential effect on weight thereafter. The 10 mg/kg dose of rapamycin resulted in a statistically similar effect as the 20 mg/kg dose (data not shown). In contrast, rapamycin-treated female Tg(PrP-A116V) mice weighed slightly more at the beginning of the measurement period, and slightly less at the end of the measurement period, but at none of the time points did this difference reach statistical significance (Fig. 1*B*). At necropsy, the mean brain weight of the entire group of rapamycin-treated Tg(PrP-A116V) mice was lower than vehicle-treated mice ($p < 0.001$) (Fig. 1*C*), but when corrected for body weight and separated by gender, this difference barely reached significance for male mice ($p = 0.0496$) and was not significant for female mice (Fig. 1*D*). All doses of rapamycin were therefore calculated for each mouse individually, based on its weight at the time of dosing.

Rapamycin delays disease onset and improves clinical phenotype of Tg(PrP-A116V) mice

Tg(PrP-A116V) mice typically exhibit normal behavior and activity until ~5 months of age, when they begin to display early signs of gait ataxia, as the primary manifestation of GSS (Yang et al., 2009). The ataxia progresses steadily, culminating in severe disability and death, typically by ~30 d. To assess the effect of rapamycin on the onset, progression, and duration of disease in these mice, we developed a scaled scoring system that ranges from A0 (no disease) to A6 (terminal). Based on this scale, the onset of disease is defined as A2, when ataxia is clearly present (see Materials and Methods for details of the ataxia assessment), and mice are killed at the end of stage A5 or the beginning of stage 6, when they are unable to appropriately feed.

The mean age at disease onset of vehicle-injected mice was 134 ± 2.6 d, which agrees well with that of untreated Tg(PrP-A116V) mice (Yang et al., 2009), suggesting the stress of injections and handling did not influence disease onset (Fig. 2*A*). The mean age of onset was significantly delayed in mice treated with rapamycin, in a dose-related manner; mice receiving 10 mg/kg rapamycin had an onset of 149 ± 3.7 d ($p = 0.05$, compared with vehicle) and those treated with 20 mg/kg had an onset of 159 ± 4.2 d ($p < 0.0001$, compared with vehicle). While these numbers reflect a 10 and 18% delay in disease onset, respectively, and reach different levels of significance, using a Bonferroni post-test analysis, they were not statistically significantly different from each other.

To assess the effect of rapamycin on the progression of disease in Tg(PrP-A116V) mice, we calculated the average disability score of mice within each treatment group at several time points, beginning at 120 d, just before the typical onset of disease, until 190 d, when the majority of vehicle-treated mice were dead. At most time points, a significant dose-related improvement in disability scores was evident, suggesting that rapamycin shifts the disability curve to the right (Fig. 2*B*). These data are also visually presented as a bar graph that displays the percentage of mice within each clinical disability stage at each time point (Fig. 2*C–E*). Rapamycin-treated mice show a predominance of lighter sections (lower disability scores), compared with vehicle-treated mice throughout the observation period. (Fig. 2*C–E*).

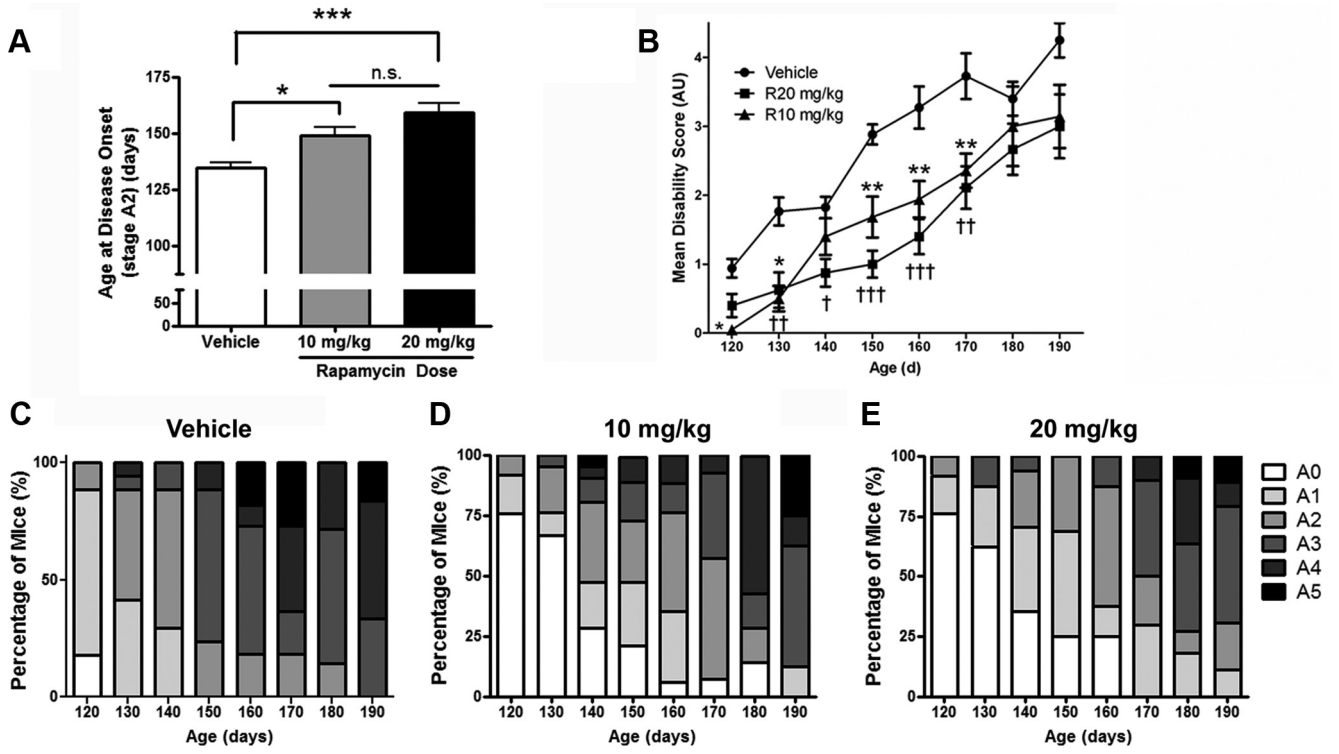

Figure 2. Rapamycin delays disease onset and progression in Tg(PrP-A116V) mice. ***A***, Mean age of disease onset ± SE (A2 stage) of mice chronically treated with vehicle or rapamycin at 10 or 20 mg/kg, beginning at 6 weeks of age. Vehicle, 134 ± 2.6 d ($n = 20$); rapamycin (10 mg/kg), 149 ± 3.7 d ($n = 24$); rapamycin (20 mg/kg), 159 ± 4.2 d ($n = 23$). *$p < 0.05$; ***$p = 0.0001$. ANOVA, Bonferroni's *post hoc* test; n.s., not significantly different. ***B***, Disease (disability) scores of Tg(PrP-A116V) mice plotted over time. Animals were assessed weekly and scored according to an ataxia/disability scale that ranges from A0 (no signs) to A5 (severely ataxic, near terminal), when they were killed. Mean disability scores ± SE are plotted. Numbers of animals per group were initially 17 (vehicle), 25 (rapamycin 10 mg/kg), and 20 for (rapamycin at 20 mg/kg), and by 190 d, remaining mice numbered 4, 8, and 8, respectively. ANOVA was used to compare the three treatment groups at each time point, followed by Bonferroni's *post hoc* test. Significant differences between vehicle and rapamycin (10 mg/kg) group are indicated by the asterisk (*). Significant differences between vehicle and rapamycin 20 mg/kg are indicated by the dagger symbol (†). One, two, and three symbols represents a $p < 0.05$, $p < 0.01$, and $p < 0.001$ level of significance compared with vehicle-treated group, respectively. Although the mean disability scores for the higher rapamycin dose were lower throughout the observation period, no significant differences ($p < 0.05$) were detected between rapamycin at 10 mg/kg and rapamycin at 20 mg/kg at any age analyzed. ***C–E***, The bars represent the percentage of mice within each stage of disease at the indicated time point. Note that rapamycin at 10 mg/kg (***D***) and 20 mg/kg (***E***) delay the appearance of higher disease scores (darker colors) compared with vehicle-treated mice (***C***).

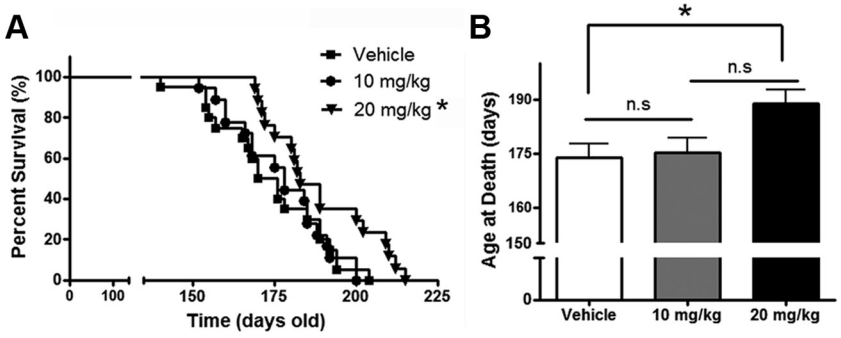

Figure 3. Rapamycin extends survival of Tg(PrP-A116V) mice. ***A***, Kaplan–Meier survival curve of mice chronically treated with vehicle or rapamycin at 10 or 20 mg/kg three times per week, beginning at 6 weeks of age. Rapamycin at 20 mg/kg, but not 10 mg/kg, significantly increased the survival of Tg(PrP-A116V) mice (*$p < 0.05$). ***B***, Mean age at death ± SE of Tg(PrP-A116V) treated with vehicle or rapamycin. Actual numbers are 173 ± 3.7 d ($n = 20$) for vehicle, 175 ± 3.8 d ($n = 19$) for 10 mg/kg rapamycin, and 189 ± 3.8 d ($n = 17$) for 20 mg/kg rapamycin (*$p < 0.05$).

Rapamycin improves survival of Tg(PrP-A116V) mice

Tg(PrP-A116V) mice are killed at the terminal clinical stage of disease (end of A5, beginning of A6), when the mice are severely disabled and no longer able to feed themselves. We compared survival times among the three treatment groups to determine whether rapamycin delays death in Tg(PrP-A116V) mice. Survival curves for each group are plotted in Figure 3*A*. A significant ($p = 0.018$) rightward shift in the survival curve was present in mice that received 20 mg/kg rapamycin, but not in those receiving 10 mg/kg ($p = 0.7$). A similar relationship was found by comparing the mean age at death of the three treatment groups. Whereas 20 mg/kg rapamycin significantly delayed the mean age at death to 189 ± 3.8 d, compared with 173 ± 3.7 d for the vehicle-treated group, the mean age at death for the 10 mg/kg dose was 175 ± 3.8 d, which did not differ from the control group (Fig. 3*B*).

Rapamycin inhibits accumulation of insoluble PrP

A biochemical feature of Tg(PrP-A116V) mice is the presence of detergent-insoluble PrP-A116V in the brain. Because this can be detected before the development of PrP plaque pathology, it suggests that insoluble misfolded PrP-A116V predates the manifestation of disease. To determine whether the improvement in clinical phenotype of rapamycin-treated mice correlates with a reduction in insoluble PrP-A116V, we compared this fraction in the brains of Tg(PrP-A116V) mice at a presymptomatic (80 d of age; stage A0) and advanced stage (stage A5) of disease. Relative to vehicle-treated

Tg(PrP-A116V) mice, rapamycin treatment was associated with a dose-related reduction in the fraction of brain-derived insoluble PrP-A116V in both presymptomatic (Fig. 4*A*) and advanced stage symptomatic (Fig. 4*B*) mice. This finding not only suggests that rapamycin acts to reduce the overall load of insoluble PrP throughout the course of disease, but that the symptoms of advanced disease develop, albeit with a notable delay, despite the significantly lower levels of insoluble PrP.

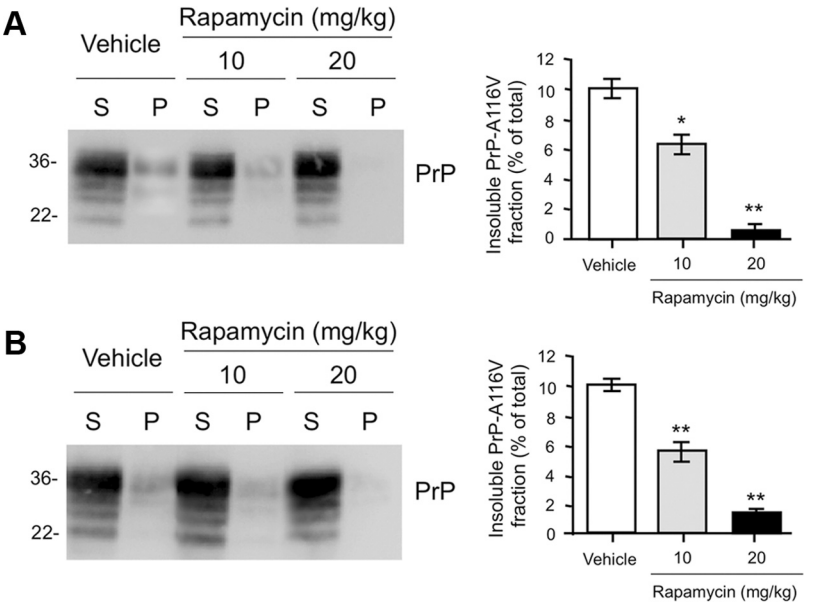

Figure 4. Rapamycin reduces the fraction of insoluble PrP-A116V. ***A***, Western blot of supernatant (S) and pellet (P) fractions of PrP-A116V prepared from brain lysates of asymptomatic (stage A0) 80-d-old Tg(PrP-A116V) mice chronically treated with vehicle or 10 or 20 mg/kg rapamycin. Sample preparation is described in Materials and Methods. The markers on left are in kilodaltons. PrP detected with SAF-32 anti-mouse PrP antibody. Densitometric signal of each fraction was semiquantified using TotalLab, and the insoluble fraction is plotted as the percentage of total (S + P) signal. Actual values for each are as follows: vehicle, 10.3 ± 1.2%; rapamycin at 10 mg/kg, 6.5 ± 1.2%; rapamycin at 20 mg/kg, 0.5 ± 0.2%. ***B***, Western blot and bar graph displays the insoluble fraction of PrP-A116V in the brains of symptomatic Tg(PrP-A116V) mice during late-stage (stage A5) disease. Actual values for each are as follows: vehicle, 10.1 ± 0.60%; rapamycin at 10 mg/kg, 5.7 ± 1.16%; rapamycin at 20 mg/kg, 1.4 ± 0.4%. The markers on left are in kilodaltons. *$p < 0.05$, **$p < 0.01$, $n = 3$ for each treatment per time point, Student's *t* test, from vehicle control. Error bars indicate SEM.

Rapamycin inhibits PrP amyloid plaque generation

The pathognomonic feature of GSS in humans, and the most prominent histopathologic feature in Tg(PrP-A116V) mice, is the deposition of PrP amyloid plaques, especially within the granular layer of the cerebellum (Yang et al., 2009). In Tg(PrP-A116V) mice, plaques are detectable by ~100 d of age and the number of plaques increase with disease progression. Because they are true amyloid, they can be detected by thioflavin S. To determine whether the reduction in insoluble PrP-A116V and mitigation of the clinical phenotype are tied to a reduction in PrP plaque deposition, we compared the plaque burden within the cerebella of mice from each treatment group at ~160 d of age, when >50% of rapamycin-treated mice were clearly symptomatic (i.e., reached stage A2). The average area of thioflavin S staining per total area of cerebellar tissue section was measured using ImageJ. Vehicle-treated Tg(PrP-A116V) mice displayed well developed and numerous plaques distributed throughout the cerebellar granule cell layer (Fig. 5*A*, top row). In stark contrast, mice treated with rapamycin were nearly or completely devoid of plaques. In mice receiving 10 mg/kg, the measured plaque area was 28.7 ± 9.6% ($n = 4$; $p < 0.01$) of that measured in vehicle-treated mice (Fig. 5*A*, second row and graph), whereas in mice receiving 20 mg/kg, no plaques were detected in any sections examined ($n = 6$) (Fig. 5*A*, bottom row and graph).

We questioned whether rapamycin delays the production of plaques in Tg(PrP-A116V) mice or it persistently suppresses the generation of plaques throughout the course of disease, as suggested by the insolubility data in Figure 4. To determine this, we examined the plaque burden within the cerebella of mice that received 20 mg/kg rapamycin and were allowed to survive to terminal stages of disease. As expected, the plaque burden of vehicle-treated mice was increased, relative to that in 160-d-old vehicle-treated mice (125.3 ± 14.1%). However, surprisingly, terminal mice treated with rapamycin were devoid of plaque deposits (Fig. 5*B* and graph). These findings not only suggests that the generation of plaques is prevented by rapamycin, but they also support the concept that plaque pathology is not required for the GSS phenotype, since rapamycin-treated mice developed ataxia and eventually reached end-stage levels of disability.

PrP expression is not affected by rapamycin

In addition to its role as an autophagy supressor, mTOR is also a master regulator of protein translation, via its downstream targets p70s6k and 4E-BP1 (Bové et al., 2011). To investigate whether the decrease in insoluble PrP-A116V and the marked reduction in plaque deposition resulted from reduced PrP expression, we analyzed the effect of each treatment on the steady-state level of PrP-A116V protein and mRNA. Western blot of detergent-extracted lysates of brain homogenate from vehicle and rapamycin-treated mice revealed comparable levels of PrP (Fig. 6*A*). Similarly, semiquantitative RT-PCR did not show a significant difference in the level of PrP-A116V transcripts among the treatment groups (Fig. 6*B*). Although a slight reduction in PrP-A116V mRNA relative to actin mRNA was present in mice treated with 10 mg/kg (92.8 ± 15.7% of baseline) and 20 mg/kg (91.4 ± 5.0% of baseline) rapamycin, these were not significantly different from vehicle-injected mice ($p > 0.05$ for both), and not likely to account for the striking reduction in plaque deposits observed in rapamycin-treated mice.

LC3 is increased in the brain of rapamycin-treated Tg(PrP-A116V) mice

To confirm that intraperitoneal administration of rapamycin was sufficient to activate autophagy within the brain of Tg(PrP-A116V) mice, we probed whole-brain lysates prepared from ~160-d-old mice for typical markers of autophagy. As shown in Figure 7*A*, LC3II, a component of the autophagosome membrane and a specific marker for autophagy activation, was significantly increased in the brains of rapamycin-treated mice relative to vehicle-treated brains. Increased levels of LC3II might reflect increased autophagosome formation or decreased autophagic flux. Because the total signal of LC3 was much greater in mice treated with rapamycin, we questioned whether rapamycin altered the expression of LC3. RT-PCR of LC3 revealed a dramatic

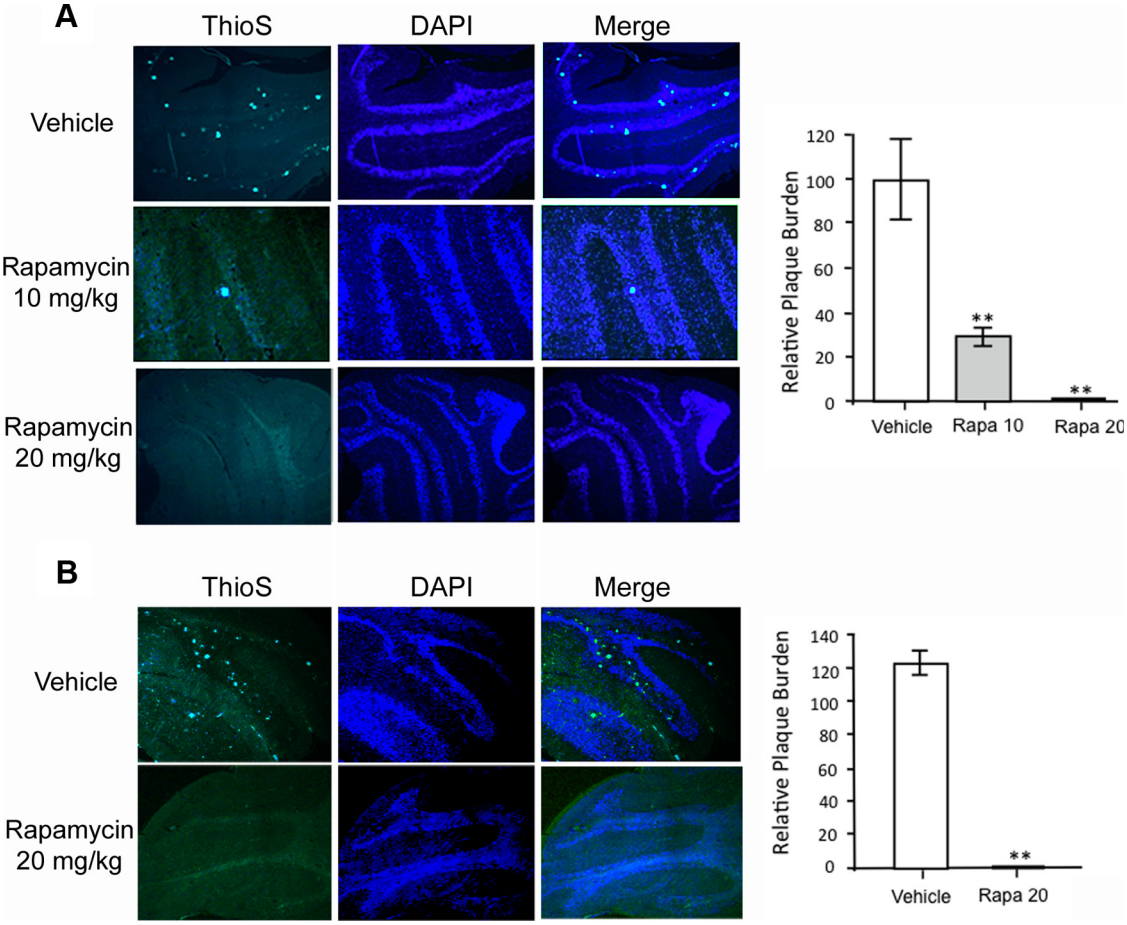

Figure 5. Rapamycin reduces PrP plaque burden in Tg(PrP-A116V) mice. ***A***, Representative cerebellar sections from ~160-d-old Tg(PrP-A116V) mice treated with vehicle or rapamycin (10 or 20 mg/kg). Sections were stained with thioflavin S to reveal PrP amyloid plaques. Nuclei were stained with DAPI. Sections were visualized by fluorescence microscopy on a Zeiss Axioplan microscope. Images are at 10× magnification. The area of thioflavin S staining, as a fraction of the total area of the cerebellar section, was determined using ImageJ and plotted as the relative plaque burden, by normalizing each group to the 160-d-old vehicle-treated group. The actual values are as follows: vehicle, 100.0 ± 36.7; rapamycin at 10 mg/kg, 28.7 ± 9.6; rapamycin at 20 mg/kg, none detected. ***B***, Representative cerebellar sections from Tg(PrP-A116V) mice in the terminal stage of disease (≥A5) following treatment with vehicle or rapamycin at 20 mg/kg and stained with thioflavin S and DAPI, as above (magnification, 10×). The relative plaque burden was determined as in ***A***, using 160-d-old vehicle-treated mice as control. The actual values are 125.3 ± 14.1 for vehicle-treated mice and none detected for rapamycin-treated mice. The bars represent the mean ± SD for each group ($n = 6$–9 samples per group). **$p < 0.01$ from vehicle treatment group, Student's *t* test.

dose-dependent increase in LC3 transcript in the brains of rapamycin-treated mice, compared with vehicle-treated controls (Fig. 7*B*). The 10 mg/kg rapamycin dose produced a ~7-fold increase in LC3 mRNA, while the 20 mg/kg dose produced a ~14-fold increase. These findings support activation of autophagy within the brain of these mice.

Rapamycin induces apoptosis in Tg(PrP-A116V) mice

During the histological assessment of these mice, we noted the presence of pyknotic nuclei in scattered cells within the cerebellar granule layer. Since rapamycin is known to induce apoptosis in cell culture, xenograft tumor models and, more recently, in mouse models of amyotrophic lateral sclerosis (ALS) (Huang et al., 2001; Tirado et al., 2005; Zhang et al., 2011), we questioned whether rapamycin treatment induced apoptosis in Tg(PrP-A116V) mice, despite its overall positive effect on disease. Apoptosis was assessed by TUNEL staining within cerebellar tissue sections adjacent to those used for assessment of plaque burden in Figures 5 and 8. The fraction of apoptotic cells was estimated as the TUNEL-positive signal relative to the signal of DAPI-stained nuclei within each tissue section, using ImageJ. In vehicle-treated mice, the fraction of TUNEL-positive cells was 1.9 ± 1.0% ($n = 7$) compared with 4.8 ± 0.6% ($n = 4$; $p < 0.01$) in mice treated with 10 mg/kg rapamycin, and 6.6 ± 3.6% ($n = 5$; $p < 0.01$ compared with vehicle, but $p = 0.42$ compared with 10 mg/kg) in mice treated with 20 mg/kg rapamycin. These data suggest the apoptosis was not dose related. To determine whether the severity of apoptosis corresponded with progression of disease, we examined a group of mice treated with 20 mg/kg rapamycin and allowed to survive to end stage. The level of apoptosis in these mice was not significantly different from that in 160-d-old mice ($p = 0.34$), and in fact, it appeared to trend downward to 4.4 ± 0.6% ($n = 3$). Thus, these findings suggest that rapamycin does induce apoptosis in our mouse model of GSS, although it does not correlate directly with dose or disease progression, at least beyond 160 d.

Rapamycin induces apoptosis in glial cells but not in neurons

We questioned the paradoxical increase in apoptosis of disease-mitigated rapamycin-treated Tg(PrP-A116V) mice. Prior work suggested that high doses or prolonged administration of rapamycin have the potential to cross-inhibit the mTOR2 complex, resulting in a reduction in Akt/PKB activity in specific cell lines (Sarbassov et al., 2006). We considered that rapamycin was in-

ducing apoptosis in a non-neuronal subpopulation of cells that are not integral to disease. To test this, we combined TUNEL staining with immunofluorescence staining with either GFAP antibody to detect glial cells, or NeuN antibody to detect neurons. Representative images from cerebellar sections of ~160-d-old mice treated with 20 mg/kg rapamycin are presented in Figure 9. TUNEL-positive nuclei were nearly completely associated with the cytoplasmic glial marker GFAP (Fig. 9*A*) and nearly completely separate from NeuN-positive nuclei (Fig. 9*B*). These results strongly suggest the enhanced apoptosis observed with rapamycin in the Tg(PrP-A116V) mice is selective for non-neuronal cells, primarily astrocytic glia.

Discussion

We show that *in vivo* inhibition of mTOR mitigates the phenotypic expression of genetic prion disease in a mouse model of GSS. Chronic treatment of Tg(PrP-A116V) mice with rapamycin significantly delayed disease onset, reduced disability, and improved survival. These clinical improvements were coincident with a reduction in the fraction of insoluble PrP-A116V and a striking reduction in PrP amyloid plaque deposits in brain.

These findings compare with those reported for other models of neurodegenerative disease (Bové et al., 2011). Rapamycin reduced the load of huntingtin aggregates and improved motor performance in a mouse model of HD (Ravikumar et al., 2004) and it reduced α-synuclein accumulation in PD transgenic mice (Crews et al., 2010). In addition, it was recently shown to improve cognitive deficits, decrease soluble Aβ, and reduce Aβ plaque burden in some (Spilman et al., 2010; Yang et al., 2011), but not all (Zhang et al., 2010), transgenic mouse models of AD.

Ours is not the first report to suggest a potential link between autophagy and prion disease. Ultrastructural evidence for autophagy was initially described in animals and then humans with prion disease (for review, see Liberski et al., 2004). Induction of autophagy in experimental models of prion disease has also been attempted, although the results have been mixed. Imatinib, a cancer drug that activates autophagy, enhanced the lysosomal degradation of PrP^{Sc}, the proteinase K (PK)-resistant pathogenic isoform of PrP, *in vitro* (Ertmer et al., 2007; Heiseke et al., 2009b) and it delayed the onset of symptoms and appearance of PrP^{Sc} in the CNS of mice peripherally inoculated with scrapie (Yun et al., 2007), while rapamycin modestly extended survival in scrapie-infected mice (Heiseke et al., 2009a). Trehalose, a novel autophagy inducer, also reduced the load of PK-resistant PrP^{Sc} in cells chronically infected with scrapie prions; however, it did not affect the course of disease in scrapie-infected mice (Aguib et al., 2009). While these studies focused on transmissible prion disease, our report provides the first evidence that rapamycin can mitigate the development of genetically induced prion disease.

Based on work in *Drosophila* that links the cytoprotective effects of rapamycin to the expression of autophagy-related genes (Berger et al., 2006; Pandey et al., 2007), autophagy induction is likely to mediate its protective effects. This is supported by the robust upregulation of LC3 and the increased conversion of LC3I to LC3II in the brains of rapamycin-treated Tg(PrP-A116V) mice. However, rapamycin does possess other properties to be

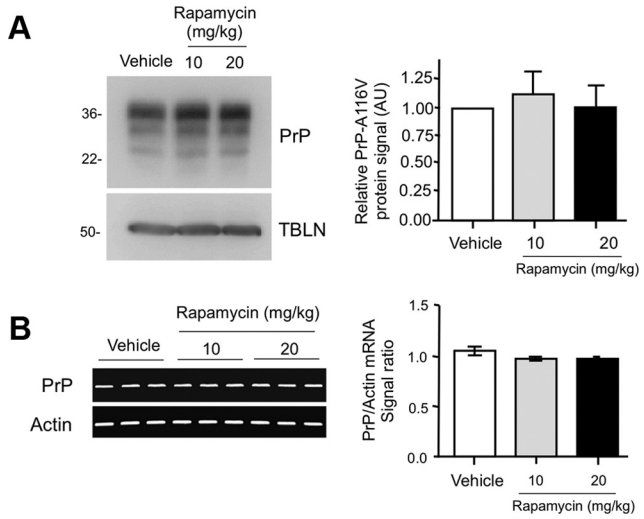

Figure 6. Rapamycin does not alter protein or transcript levels of PrP. ***A***, Western blot comparing PrP levels in total brain lysates prepared from ~160-d-old Tg(PrP-A116V) mice chronically treated with vehicle or rapamycin at 10 or 20 mg/kg. Tubulin (TBLN) represents a loading control. The markers on the left are in kilodaltons. Densitometry quantification ± SD of PrP signal with each dose of rapamycin relative to vehicle was determined using ImageJ software and is plotted in the adjacent graph. No significant difference was detected among the three groups (ANOVA). ***B***, RT-PCR of PrP-A116V and actin (control) transcripts from mice chronically administered vehicle or rapamycin at 10 or 20 mg/kg. The adjacent graph displays the ratio of PrP transcript signal ± SD relative to actin signal for each treatment group ($n = 3$ mice per experiment). No significant differences were detected by ANOVA.

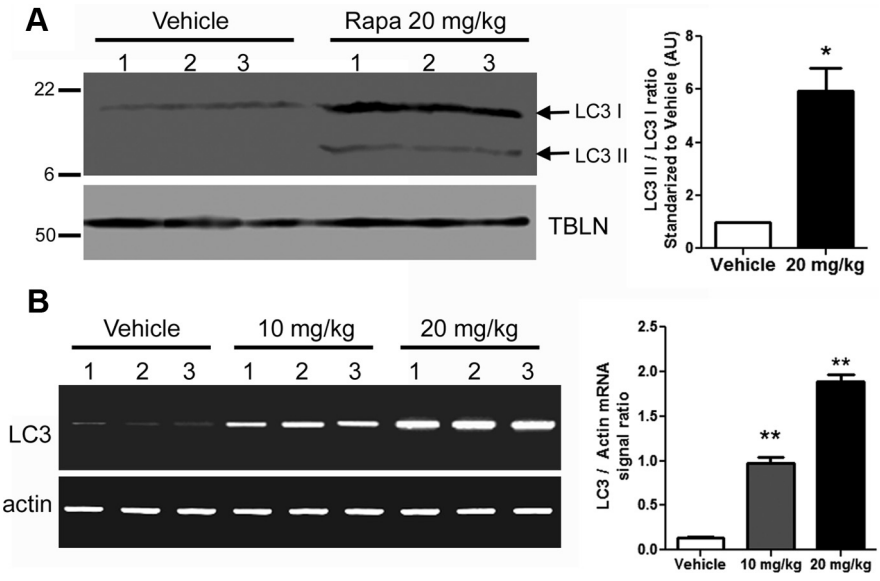

Figure 7. LC3II levels and LC3 transcripts are increased in the CNS of rapamycin-treated Tg(PrP-A116V) mice. ***A***, Representative Western blot prepared from brain lysates of ~160-d-old mice chronically treated with vehicle or rapamycin (Rapa) at 20 mg/kg, and probed for LC3. Tubulin (TBLN) is a loading control. Each sample represents 30 μg of total protein. The markers on the left are in kilodaltons. The adjacent bar graph displays the ratio of LC3II/LC3I densitometric signal, as determined by ImageJ, relative to that of vehicle-treated mice ($n = 3$ mice for each treatment). ***B***, RT-PCR of LC3 mRNA from the brains of ~160-d-old mice chronically treated with vehicle or rapamycin at 10 or 20 mg/kg. RT-PCR of actin mRNA is presented as a reference control. Adjacent bar graph presents the ratio of LC3/actin RT-PCR signal for each treatment ($n = 3$ for each). *$p < 0.05$; **$p < 0.001$. Error bars indicate SEM.

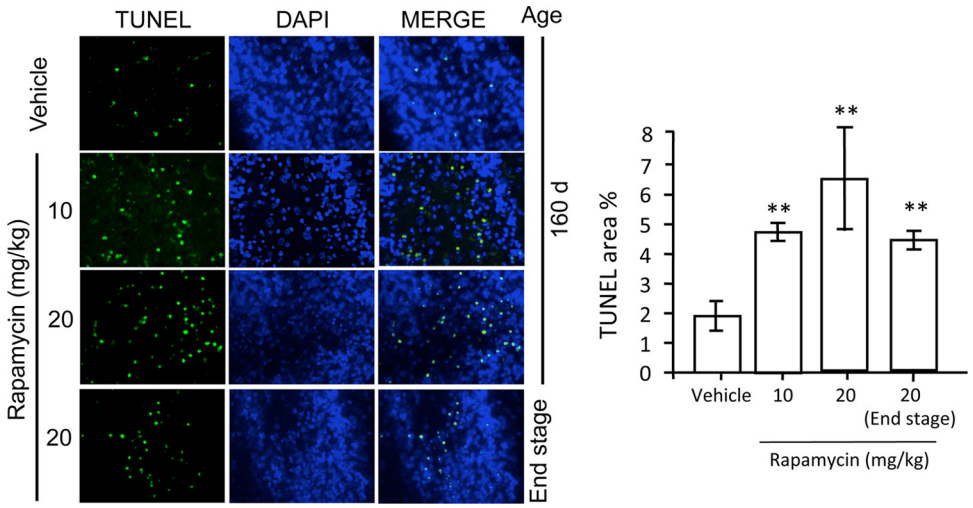

Figure 8. Rapamycin induces apoptosis in the CNS of Tg(PrP-A116V) mice. TUNEL (green) and DAPI staining of representative cerebella of 160-d-old and end-stage (A5) Tg(PrP-A116V) mice chronically treated with vehicle or rapamycin at 10 or 20 mg/kg. Cerebellar sections adjacent to those used for assessment of plaque burden in Figure 5 were used to assess apoptosis. Adjacent bar graph displays the ratio of TUNEL-positive area relative to the total neuron load, as estimated by DAPI signal area, using ImageJ software. The bars represent the mean ± SE ($n = 6$ mice per group). $^{**}p < 0.01$, significantly different from vehicle, Student's *t* test. No statistical differences were detected between any rapamycin-treated groups at 160 d compared with end-stage time points, suggesting this feature did not progress with disease.

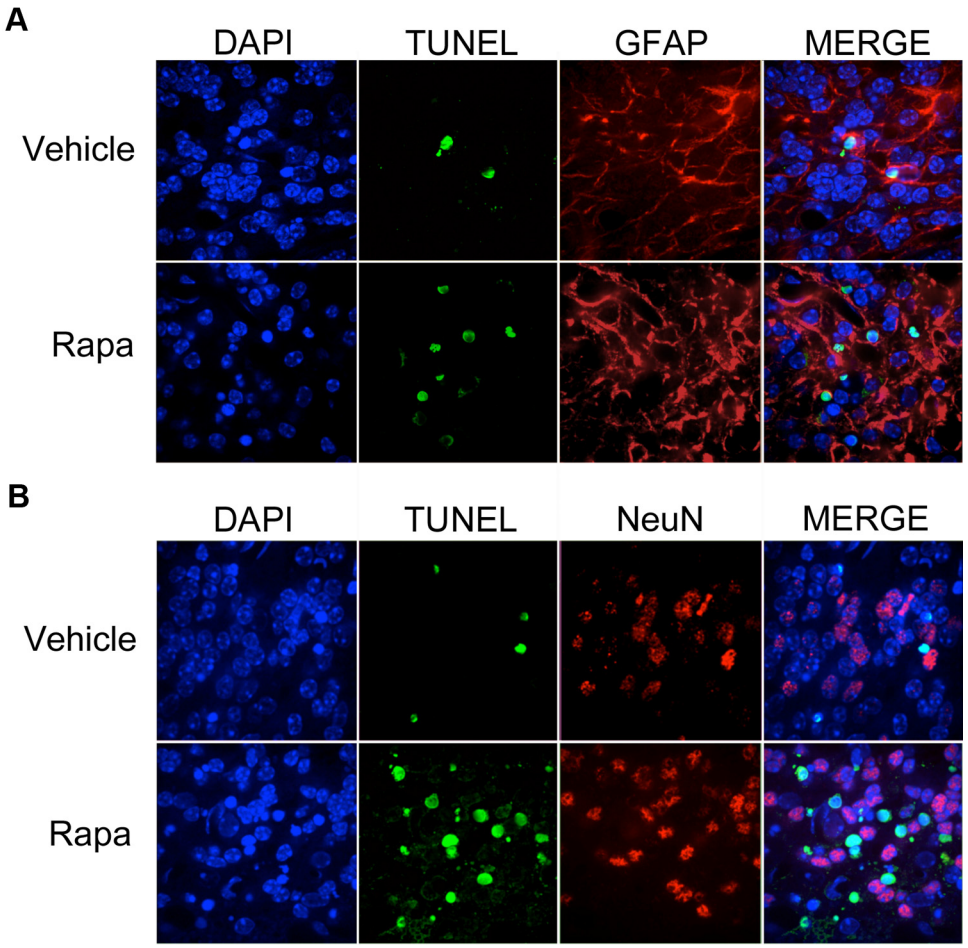

Figure 9. Apoptosis induced by rapamycin is selective for astrocytes. ***A***, ***B***, Cerebellar sections from mice treated with 20 mg/kg rapamycin (Rapa) were costained for TUNEL (green) and either rabbit anti-GFAP antibody (***A***), to detect astrocytes, or mouse anti-NeuN monoclonal antibody (***B***), to detect nuclei of neuronal cells. TUNEL-positive nuclei (green) were associated primarily within GFAP-positive cells, although the difference in subcellular localization of the two markers made it difficult to rule out an effect on neuronal cells. NeuN staining (***B***) of neuronal nuclei confirmed a nearly complete absence of colocalization with TUNEL staining. Of 200 NeuN-positive neurons, only 11 were found to be TUNEL positive. These data suggest the enhanced apoptosis of rapamycin was selective for astrocytes and not neurons.

considered. Its potent immunosuppressive action (Huang et al., 2003) could theoretically affect prion disease. The immune system, especially follicular dendritic cells, participates in the delivery of prions from the periphery to the CNS (Prinz et al., 2002; Aguzzi et al., 2003). However, spontaneous and genetic prion diseases, which originate in the CNS, lack a typical immune response and the lymphoreticular system does not appear to play a role. Thus, while the immunosuppressive feature of rapamycin might play a role in models of peripheral scrapie infection, it is not likely to contribute to the beneficial effect observed in Tg(PrP-A116V) mice. Another important effect of rapamycin is suppression of protein translation through inhibition of mTOR (Sarbassov et al., 2005). King et al. (2008) determined that this feature, rather than autophagy-induced clearance, accounted for the reduction of insoluble huntingtin in a cell-based model of HD. We found that neither PrP-A116V mRNA transcripts nor steady-state protein levels were significantly affected by rapamycin treatment, suggesting this was not the mechanism for its beneficial effect in our mice.

Although total levels of PrP-A116V were not significantly affected, rapamycin selectively reduced the insoluble fraction of PrP-A116V. Because this was evident during the late symptomatic and presymptomatic phases of disease, we speculate that rapamycin limits production, facilitates elimination, or sequesters misfolded PrP away from the pathway that would otherwise contribute to the generation of extracellular PrP plaques. This argument is strengthened by the dramatic reduction in plaque burden observed in rapamycin-treated mice. At ~160 d of age, when PrP plaques are normally plentiful, they were barely detectable in mice that received the 10 mg/kg dose, while virtually none were detectable in mice that received the 20 mg/kg dose. Remarkably, plaque pathology was also absent in terminal stage mice treated with rapamycin, suggesting it acts to eliminate plaque production rather than simply delay their development. This has important implications with respect to the underlying pathogenesis of GSS. PrP amyloid plaques are an invariant feature of GSS that distinguishes it from other prion disease subtypes, and their presence is required for the histopathological diagnosis of GSS (for review, see Mastrianni, 2010). Whether plaque pathology contributes to the phenotypic expression of GSS has long been questioned. Our results show that, despite the absence of plaques in rapamycin-treated mice, the course of disease, although delayed, was phenotypically similar to that of untreated mice. These results complement those in transgenic mice that express PrP lacking the glycosylphosphatidylinositol (GPI) anchor and develop abundant extracellular PrP plaques, but no obvious phenotype (Chesebro et al., 2005). Our findings clearly demonstrate that plaque pathology is not essential for the expression of GSS, and the pathogenesis of GSS must be linked to a feature that precedes or parallels plaque deposition.

Unlike most neurodegenerative proteins that produce cytosolic aggregates susceptible to clearance by rapamycin-induced macroautophagy, PrP is a GPI-anchored protein that follows the secretory pathway to the plasma membrane (Campana et al., 2005). Plaques in Tg(PrP-A116V) mice appear to be comprised of full-length PrP-A116V molecules (Yang et al., 2009), suggesting it is cleaved from the plasma membrane at the GPI anchor, or secreted, as in PrP(GPI-) mice (Chesebro et al., 2005). Where autophagy might specifically function in this pathway is, as yet, unclear. However, because PrP carrying familial mutations is known to misfold within the ER, and our findings support a reduction in misfolded PrP during the presymptomatic phase, we speculate that autophagy might act to eliminate misfolded PrP that accumulates within this compartment, as an early quality control mechanism, as has been reported with α1-antitrypsin z mutant (Teckman and Perlmutter, 2000; Kamimoto et al., 2006), vasopressin (Castino et al., 2005), and dysferlin (Fujita et al., 2007). In addition, we acknowledge that an additional nonautophagic mechanism contributing to the effect of rapamycin cannot be completely ruled out.

Despite the overall beneficial effect of rapamycin, we detected an increase in apoptosis within the cerebellum, as assessed by TUNEL staining. Interestingly, this effect was not related to the dose of rapamycin, nor did it correlate with disease progression, since it did not significantly increase at end stage, compared with the 160 d time point. This paradox was initially difficult to explain. Although a reduction in PrP^C is predicted to have an apoptotic effect, based on its known antiapoptotic effect against serum deprivation (Kuwahara et al., 1999) and Bax-mediated cell death (Bounhar et al., 2001; Roucou et al., 2003), Tg(PrP-A116V) mice express only mutated PrP, the levels of which were not significantly affected by rapamycin. Prior reports suggested rapamycin can induce apoptosis in several cell lines and xenograft tumor models (Huang et al., 2001; Tirado et al., 2005), and in a transgenic mouse model of ALS, it induced apoptosis within the spinal cord with associated acceleration of motor neuron disease, manifested as enhanced motor dysfunction (Zhang et al., 2011). However, our mice exhibited improvement in all disease measures, which led us to consider that non-neuronal cells might be selectively affected and, therefore, not contribute to disease manifestation. In fact, costaining cerebellar sections with TUNEL and markers for neurons or glia revealed astrocytes to be the predominant cell type undergoing apoptosis. Although this finding helps to resolve the paradoxical increase in CNS apoptosis with an improvement in clinical and histopathological features, the etiology of glial cell apoptosis is, as yet, unclear. Whether this is a direct result of long-duration rapamycin treatment, or it is directly linked to the expression of PrP-A116V, is currently under study.

In summary, we provide the first evidence for a therapeutic benefit of rapamycin in a genetic model of prion disease. To our knowledge, all prion disease therapies have been tested using models of scrapie infection. An array of therapies has been tested, with mixed results, including aggregate-inhibiting compounds, antimalarial dugs, β-sheet breaker peptides, and immunotherapy (for review, see Trevitt and Collinge, 2006; Aguzzi and O'Connor, 2010), in addition to the limited studies of autophagy-inducing drugs noted above. A consistent finding among these studies is that initiation of treatment before, or simultaneously with, prion inoculation, predicts a better response. Genetic screening in advance of disease onset can identify individuals at risk for inherited prion diseases, which makes this group ideally suited for preventative therapies that delay the onset of disease. Based on our results, the benefit for human carriers of the PrP-A117V mutation could be substantial; the 18% delay in onset observed in GSS mice could translate to at least a 7 year delay in a carrier of a GSS mutation who would normally develop the disease by age 40. Because rapamycin and its analogs are already approved for use in humans, their application to prion disease could be quickly adapted.

References

Aguib Y, Heiseke A, Gilch S, Riemer C, Baier M, Schätzl HM, Ertmer A (2009) Autophagy induction by trehalose counteracts cellular prion infection. Autophagy 5:361–369.

Aguzzi A, O'Connor T (2010) Protein aggregation diseases: pathogenicity and therapeutic perspectives. Nat Rev Drug Discov 9:237–248.

Aguzzi A, Heppner FL, Heikenwalder M, Prinz M, Mertz K, Seeger H, Glatzel

M (2003) Immune system and peripheral nerves in propagation of prions to CNS. Br Med Bull 66:141–159.
Berger Z, Ravikumar B, Menzies FM, Oroz LG, Underwood BR, Pangalos MN, Schmitt I, Wullner U, Evert BO, O'Kane CJ, Rubinsztein DC (2006) Rapamycin alleviates toxicity of different aggregate-prone proteins. Hum Mol Genet 15:433–442.
Bounhar Y, Zhang Y, Goodyer CG, LeBlanc A (2001) Prion protein protects human neurons against Bax-mediated apoptosis. J Biol Chem 276: 39145–39149.
Bové J, Martínez-Vicente M, Vila M (2011) Fighting neurodegeneration with rapamycin: mechanistic insights. Nat Rev Neurosci 12:437–452.
Campana V, Sarnataro D, Zurzolo C (2005) The highways and byways of prion protein trafficking. Trends Cell Biol 15:102–111.
Castino R, Davies J, Beaucourt S, Isidoro C, Murphy D (2005) Autophagy is a prosurvival mechanism in cells expressing an autosomal dominant familial neurohypophyseal diabetes insipidus mutant vasopressin transgene. FASEB J 19:1021–1023.
Chesebro B, Trifilo M, Race R, Meade-White K, Teng C, LaCasse R, Raymond L, Favara C, Baron G, Priola S, Caughey B, Masliah E, Oldstone M (2005) Anchorless prion protein results in infectious amyloid disease without clinical scrapie. Science 308:1435–1439.
Crews L, Spencer B, Desplats P, Patrick C, Paulino A, Rockenstein E, Hansen L, Adame A, Galasko D, Masliah E (2010) Selective molecular alterations in the autophagy pathway in patients with Lewy body disease and in models of alpha-synucleinopathy. PLoS One 5:e9313.
Ertmer A, Huber V, Gilch S, Yoshimori T, Erfle V, Duyster J, Elsässer HP, Schätzl HM (2007) The anticancer drug imatinib induces cellular autophagy. Leukemia 21:936–942.
Fornai F, Longone P, Cafaro L, Kastsiuchenka O, Ferrucci M, Manca ML, Lazzeri G, Spalloni A, Bellio N, Lenzi P, Modugno N, Siciliano G, Isidoro C, Murri L, Ruggieri S, Paparelli A (2008) Lithium delays progression of amyotrophic lateral sclerosis. Proc Natl Acad Sci U S A 105:2052–2057.
Fujita E, Kouroku Y, Isoai A, Kumagai H, Misutani A, Matsuda C, Hayashi YK, Momoi T (2007) Two endoplasmic reticulum-associated degradation (ERAD) systems for the novel variant of the mutant dysferlin: ubiquitin/proteasome ERAD(I) and autophagy/lysosome ERAD(II). Hum Mol Genet 16:618–629.
Heiseke A, Aguib Y, Riemer C, Baier M, Schätzl HM (2009a) Lithium induces clearance of protease resistant prion protein in prion-infected cells by induction of autophagy. J Neurochem 109:25–34.
Heiseke A, Aguib Y, Schatzl HM (2009b) Autophagy, prion infection and their mutual interactions. Curr Issues Mol Biol 12:87–97.
Huang S, Liu LN, Hosoi H, Dilling MB, Shikata T, Houghton PJ (2001) p53/p21(CIP1) cooperate in enforcing rapamycin-induced G_1 arrest and determine the cellular response to rapamycin. Cancer Res 61:3373–3381.
Huang S, Bjornsti MA, Houghton PJ (2003) Rapamycins: mechanism of action and cellular resistance. Cancer Biol Ther 2:222–232.
Kamimoto T, Shoji S, Hidvegi T, Mizushima N, Umebayashi K, Perlmutter DH, Yoshimori T (2006) Intracellular inclusions containing mutant alpha1-antitrypsin Z are propagated in the absence of autophagic activity. J Biol Chem 281:4467–4476.
King MA, Hands S, Hafiz F, Mizushima N, Tolkovsky AM, Wyttenbach A (2008) Rapamycin inhibits polyglutamine aggregation independently of autophagy by reducing protein synthesis. Mol Pharmacol 73:1052–1063.
Kuwahara C, Takeuchi AM, Nishimura T, Haraguchi K, Kubosaki A, Matsumoto Y, Saeki K, Matsumoto Y, Yokoyama T, Itohara S, Onodera T (1999) Prions prevent neuronal cell-line death. Nature 400:225–226.
Liberski PP, Sikorska B, Bratosiewicz-Wasik J, Gajdusek DC, Brown P (2004) Neuronal cell death in transmissible spongiform encephalopathies (prion diseases) revisited: from apoptosis to autophagy. Int J Biochem Cell Biol 36:2473–2490.
Mastrianni JA (2010) The genetics of prion diseases. Genet Med 12:187–195.
Nixon RA (2007) Autophagy, amyloidogenesis and Alzheimer disease. J Cell Sci 120:4081–4091.
Noda T, Ohsumi Y (1998) Tor, a phosphatidylinositol kinase homologue, controls autophagy in yeast. J Biol Chem 273:3963–3966.
Pandey UB, Nie Z, Batlevi Y, McCray BA, Ritson GP, Nedelsky NB, Schwartz SL, DiProspero NA, Knight MA, Schuldiner O, Padmanabhan R, Hild M, Berry DL, Garza D, Hubbert CC, Yao TP, Baehrecke EH, Taylor JP (2007) HDAC6 rescues neurodegeneration and provides an essential link between autophagy and the UPS. Nature 447:859–863.
Prinz M, Montrasio F, Klein MA, Schwarz P, Priller J, Odermatt B, Pfeffer K, Aguzzi A (2002) Lymph nodal prion replication and neuroinvasion in mice devoid of follicular dendritic cells. Proc Natl Acad Sci U S A 99:919–924.
Prusiner SB (1998) Prions. Proc Natl Acad Sci U S A 95:13363–13383.
Ravikumar B, Duden R, Rubinsztein DC (2002) Aggregate-prone proteins with polyglutamine and polyalanine expansions are degraded by autophagy. Hum Mol Genet 11:1107–1117.
Ravikumar B, Vacher C, Berger Z, Davies JE, Luo S, Oroz LG, Scaravilli F, Easton DF, Duden R, O'Kane CJ, Rubinsztein DC (2004) Inhibition of mTOR induces autophagy and reduces toxicity of polyglutamine expansions in fly and mouse models of Huntington disease. Nat Genet 36:585–595.
Ross CA, Poirier MA (2004) Protein aggregation and neurodegenerative disease. Nat Med 10 [Suppl]:S10–S17.
Roucou X, Guo Q, Zhang Y, Goodyer CG, LeBlanc AC (2003) Cytosolic prion protein is not toxic and protects against Bax-mediated cell death in human primary neurons. J Biol Chem 278:40877–40881.
Sarbassov DD, Ali SM, Sabatini DM (2005) Growing roles for the mTOR pathway. Curr Opin Cell Biol 17:596–603.
Sarbassov DD, Ali SM, Sengupta S, Sheen JH, Hsu PP, Bagley AF, Markhard AL, Sabatini DM (2006) Prolonged rapamycin treatment inhibits mTORC2 assembly and Akt/PKB. Mol Cell 22:159–168.
Sarkar S, Davies JE, Huang Z, Tunnacliffe A, Rubinsztein DC (2007) Trehalose, a novel mTOR-independent autophagy enhancer, accelerates the clearance of mutant huntingtin and alpha-synuclein. J Biol Chem 282:5641–5652.
Schmelzle T, Hall MN (2000) TOR, a central controller of cell growth. Cell 103:253–262.
Spilman P, Podlutskaya N, Hart MJ, Debnath J, Gorostiza O, Bredesen D, Richardson A, Strong R, Galvan V (2010) Inhibition of mTOR by rapamycin abolishes cognitive deficits and reduces amyloid-beta levels in a mouse model of Alzheimer's disease. PLoS One 5:e9979.
Teckman JH, Perlmutter DH (2000) Retention of mutant alpha(1)-antitrypsin Z in endoplasmic reticulum is associated with an autophagic response. Am J Physiol Gastrointest Liver Physiol 279:G961–G974.
Tirado OM, Mateo-Lozano S, Notario V (2005) Rapamycin induces apoptosis of JN-DSRCT-1 cells by increasing the Bax:Bcl-xL ratio through concurrent mechanisms dependent and independent of its mTOR inhibitory activity. Oncogene 24:3348–3357.
Trevitt CR, Collinge J (2006) A systematic review of prion therapeutics in experimental models. Brain 129:2241–2265.
Walpoth BH, Pavlicek M, Celik B, Nicolaus B, Schaffner T, Althaus U, Hess OM, Carrel T, Morris RE (2001) Prevention of neointimal proliferation by immunosuppression in synthetic vascular grafts. Eur J Cardiothorac Surg 19:487–492.
Webb JL, Ravikumar B, Atkins J, Skepper JN, Rubinsztein DC (2003) Alpha-Synuclein is degraded by both autophagy and the proteasome. J Biol Chem 278:25009–25013.
Williams A, Jahreiss L, Sarkar S, Saiki S, Menzies FM, Ravikumar B, Rubinsztein DC (2006) Aggregate-prone proteins are cleared from the cytosol by autophagy: therapeutic implications. Curr Top Dev Biol 76:89–101.
Yang DS, Stavrides P, Mohan PS, Kaushik S, Kumar A, Ohno M, Schmidt SD, Wesson D, Bandyopadhyay U, Jiang Y, Pawlik M, Peterhoff CM, Yang AJ, Wilson DA, St George-Hyslop P, Westaway D, Mathews PM, Levy E, Cuervo AM, Nixon RA (2011) Reversal of autophagy dysfunction in the TgCRND8 mouse model of Alzheimer's disease ameliorates amyloid pathologies and memory deficits. Brain 134:258–277.
Yang W, Cook J, Rassbach B, Lemus A, DeArmond SJ, Mastrianni JA (2009) A new transgenic mouse model of Gerstmann-Straussler-Scheinker syndrome caused by the A117V mutation of PRNP. J Neurosci 29:10072–10080.
Yun SW, Ertmer A, Flechsig E, Gilch S, Riederer P, Gerlach M, Schätzl HM, Klein MA (2007) The tyrosine kinase inhibitor imatinib mesylate delays prion neuroinvasion by inhibiting prion propagation in the periphery. J Neurovirol 13:328–337.
Zhang S, Salemi J, Hou H, Zhu Y, Mori T, Giunta B, Obregon D, Tan J (2010) Rapamycin promotes beta-amyloid production via ADAM-10 inhibition. Biochem Biophys Res Commun 398:337–341.
Zhang X, Li L, Chen S, Yang D, Wang Y, Zhang X, Wang Z, Le W (2011) Rapamycin treatment augments motor neuron degeneration in SOD1(G93A) mouse model of amyotrophic lateral sclerosis. Autophagy 7:412–425.